Luminescence of Ce^{3+} at two different sites in α-$Sr_2P_2O_7$ under vacuum ultraviolet-UV and x-ray excitation

Dejian Hou,[1] Bing Han,[1] Wanping Chen,[1] Hongbin Liang,[1,a)] Qiang Su,[1] Pieter Dorenbos,[2] Yan Huang,[3] Zhenhua Gao,[3] and Ye Tao[3]

[1]*MOE Laboratory of Bioinorganic and Synthetic Chemistry, State Key Laboratory of Optoelectronic Materials and Technologies, School of Chemistry and Chemical Engineering, Sun Yat-sen University, Guangzhou 510275, China*

[2]*Faculty of Applied Sciences, Delft University of Technology, Mekelweg 15, 2629 JB Delft, The Netherlands*

[3]*Beijing Synchrotron Radiation Facilities, Institute of High Energy Physics, Chinese Academy of Sciences, Beijing 100039, China*

(Received 3 June 2010; accepted 10 September 2010; published online 26 October 2010)

A series of Ce^{3+} doped α-$Sr_{2-2x}Ce_xNa_xP_2O_7$ phosphor compounds has been prepared using a high-temperature solid-state reaction technique. The luminescence properties under vacuum ultraviolet-UV and x-ray excitation were studied. Luminescence spectra reveal three UV-emitting peaks at about 310, 330, and 350 nm from which we conclude that Ce^{3+} occupies two distinct sites in α-$Sr_2P_2O_7$. The influences of the doping concentration, the temperature, and the excitation wavelength on the luminescence of Ce^{3+} at the Ce(I) and Ce(II) sites together with the decay characteristics are discussed. The light yield under x-ray excitation is found to be around 10 000 photons/MeV. © *2010 American Institute of Physics*. [doi:10.1063/1.3500333]

I. INTRODUCTION

Ce^{3+} is one of the lanthanide ions that shows $4f-5d$ transitions in the UV or visible part of the spectrum. The $5d$ orbital is an outer orbital of the lanthanide and its crystalline environment has strong influence on the energies of the $5d$ states. Consequently the $4f-5d$ transitions appear at wavelengths that depend strongly on both the kind of lanthanide ion and the host lattice. The investigation on the $4f-5d$ transitions of Ce^{3+} gives information that can be used to predict the $5d$ transitions of other lanthanide ions in the same host lattice.[1] Because the $4f-5d$ transitions are dipole-allowed, they have a large optical absorption cross-section relative to the dipole-forbidden $4f-4f$ transition. Furthermore because of the strong $5d$-electron–lattice or electron–phonon interaction, the $4f-5d$ transitions appear as broad bands in spectra. The luminescence of inorganic phosphors based on lanthanide $4f-5d$ transitions has been extensively investigated, and phosphors are used for many applications.[2–6] For example, $Y_3Al_5O_{12}:Ce^{3+}$ is commonly used as a yellow-emitting component in InGaN/GaN-based light emitting diodes, $Y_2SiO_5:Ce^{3+}$ is recommended to be a potential blue-emitting phosphor in field emission displays, and $Lu_2SiO_5:Ce^{3+}$ is a commercially available scintillator in medical imaging detectors for positron emission tomography (PET) systems. In particular, for application in new time-of-flight PET scanners, novel lanthanide-doped scintillation materials with faster luminescence are required.[7]

The alpha-phase of strontium pyrophosphate α-$Sr_2P_2O_7$ is an important host for luminescence of lanthanides and transition metals.[8–10] In this paper, the luminescence properties of Ce^{3+} doped α-$Sr_2P_2O_7$ is investigated. The average energy (centroid) of the Ce^{3+} $5d$ levels are expected to undergo a small shift in pyrophosphate compounds because oxygen ligands are strongly bonded and the related properties like nephelauxetic effect, ligand polarizability, and covalency between ligands and Ce^{3+} are small.[1] As a result, the emission of Ce^{3+} is expected at short-wavelength, and because decay scales with the third power of emission wavelength, with a fast decay.[1,8]

II. EXPERIMENTAL

Powder samples of $Sr_{2-2x}Ce_xNa_xP_2O_7$ (x =0.005, 0.01, 0.02, 0.03, 0.04, 0.05) were synthesized by a traditional high-temperature solid-state reaction route. Na^+ was added as a charge compensator. The reactants were $SrCO_3$ [analytical reagent (A.R.)], $(NH_4)_2HPO_4$ (A.R.), CeO_2 (99.99%), and Na_2CO_3 (A.R.). The chemical reactions are as follow:

$$(4-4x)SrCO_3 + 4(NH_4)_2HPO_4 + 2xCeO_2 + xNa_2CO_3 + xCO \xrightarrow{450\,^\circ C/1.5\ h,\ 1100\,^\circ C/2\ h} 2Sr_{2(1-x)}Ce_xNa_xP_2O_7 + (4-2x)CO_2 + 6H_2O + 8NH_3.$$

After mixing and thoroughly grinding, the stoichiometric mixtures were first preheated at 450 °C for 90 min in ambient air and then slowly cooled down. After preheated, they were reground and sintered at 1100 °C for 2 h in thermal-carbon reducing atmosphere. The final products were cooled to room temperature (RT) by switching off the muffle furnace and ground into white powders. The structure of the samples was examined by powder x-ray diffraction (XRD) with Cu $K\alpha$ radiation on a Rigaku D/max 2200 X-Ray Diffractometer operating at 40 kV and 30 mA.

The steady-state (excitation and emission) spectra in the UV range were measured with a FLS920 spectrometer equipped with a CTI-cryogenics temperature controlling sys-

a)Electronic mail: cesbin@mail.sysu.edu.cn.

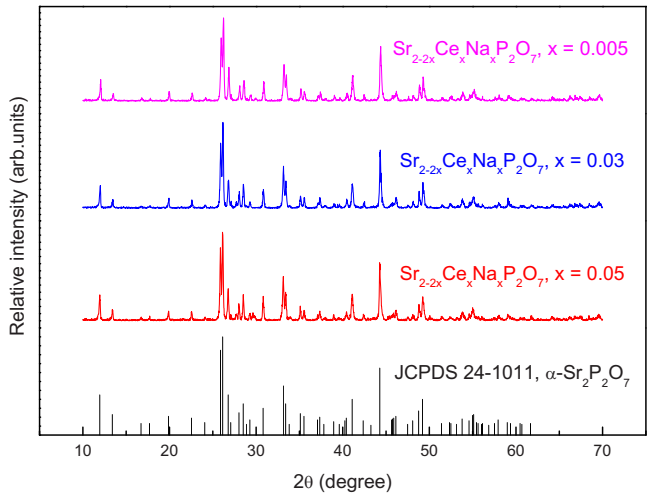

FIG. 1. (Color online) Powder XRD patterns of α-$Sr_{2-2x}Ce_xNa_xP_2O_7$ (x =0.005,0.03,0.05) at RT.

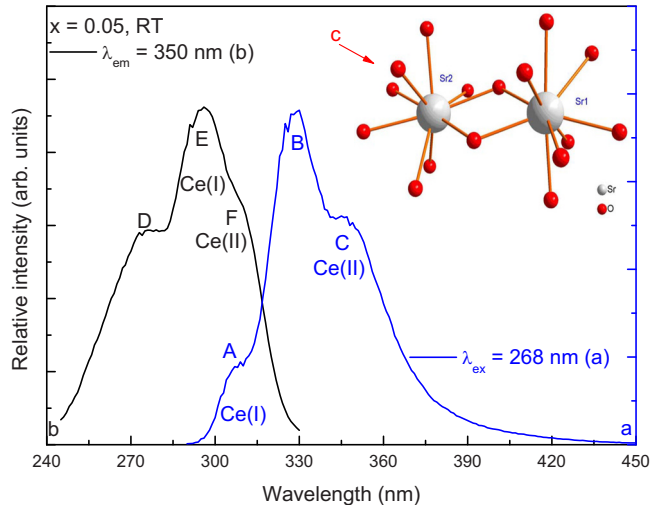

FIG. 2. (Color online) The emission (λ_{ex}=268 nm, (a) and excitation (λ_{em}=350 nm, (b) spectra of α-$Sr_{1.90}Ce_{0.05}Na_{0.05}P_2O_7$ at RT, and (c) the coordination around Sr1 and Sr2 sites in α-$Sr_2P_2O_7$.

tem, and a 450 W xenon lamp was used as the excitation source. The decay curves were recorded on an Edinburgh FLSP920 spectrometer where with excitation photons from a 150 W nF900 ns flash lamp with a pulse width of 1 ns and pulse repetition rate of 40–100 kHz. The vacuum ultraviolet (VUV) excitation and corresponding luminescence spectra were measured at the VUV spectroscopy experimental station on beam line 4B8 of Beijing Synchrotron Radiation Facility (BSRF). The measurement details have been described elsewhere.[11] X-ray excited emission spectra were recorded by facilities at Delft University of Technology, the Netherlands. Further measurement details can be found in our previous work.[12]

III. RESULTS AND DISCUSSION

A. Powder XRD

Strontium pyrophosphate $Sr_2P_2O_7$ is known to be polymorphic. The low-temperature β-phase is tetragonal, while the high-temperature α-phase is orthorhombic.[13–15] The high-temperature modification has the centrosymmetric *Pnam* space group. The XRD patterns of the powder samples α-$Sr_{2-2x}Ce_xNa_xP_2O_7$ (x=0.005,0.01,0.02,0.03,0.04,0.05) were measured at RT, and as examples three diffractograms for the samples with x=0.005,0.03,0.05 are shown in Fig. 1. The diffractograms for all the samples are similar and agree well with Joint Committee for Powder Diffraction Standard file 24-1011 (α-$Sr_2P_2O_7$), indicating that all samples are of single pure phase. The substitution of Sr^{2+} by Ce^{3+} and by the charge compensating codopant Na^+ does not significantly influence the crystal structure. When the doping content is above x=0.05, we could not obtain a single pure phase anymore. Therefore, only the spectra for the samples with doping concentration $x \leq 0.05$ are presented and discussed in this work.

B. Evidence that Ce^{3+} occupies two different lattice sites

The emission (λ_{ex}=268 nm, curve a) and excitation (λ_{em}=350 nm, curve b) spectra of α-$Sr_{1.90}Ce_{0.05}Na_{0.05}P_2O_7$ measured at RT are shown in Fig. 2. Three broad emission bands A (~307 nm), B (~327 nm), and C (~350 nm) that are attributed to $5d^1 \rightarrow 4f^1$ transitions of Ce^{3+} in the host lattice are observed in Fig. 2(a). Usually, a doublet band emission is observed when Ce^{3+} ions are at one specific lattice site due to the transitions from the relaxed lowest $5d$ excited state to the $^2F_{5/2}$ and $^2F_{7/2}$ spin-orbit split $4f$ ground states. The energy separation of the two emission bands is then about 2000 cm^{-1}. However, we observe three bands in the emission spectrum upon 268 nm excitation. This indicates that Ce^{3+} ions enter more than one distinct site in α-$Sr_2P_2O_7$.

In α-$Sr_2P_2O_7$, each Sr^{2+} cation is coordinated by nine O^{2-} anions belonging to five different pyrophosphate groups. These Sr^{2+} cation sites can be divided into two different types. In both cases Sr^{2+} is at the center of a quite similar SrO_9 polyhedron as shown in Fig. 2(c). Both polyhedra can be derived from a cube. Six oxygen atoms are close to six corners of the cube, which define three edges in the y direction of the structure. The other three O^{2-} are very roughly arranged along the fourth parallel cube edge. Both sites have C_s symmetry but the site sizes are slightly different. The $Sr1^{2+}$ ion has the largest site size with average distance of 0.2721 nm for the Sr1–O bonds. The average distance is about 0.2679 nm for the Sr2–O bonds.[15] Because the energy difference between band A (~307 nm) and band B (~327 nm) is about 2000 cm^{-1}, they may be attributed to the emission of Ce^{3+} at one specific lattice site, which we marked as the Ce(I) site. Since the energy difference between band B and band C is also ~2000 cm^{-1}, we assign those bands to Ce^{3+} at the Ce(II) site. In the above assignment we therefore claim that band B is the superposition of the $5d \rightarrow {}^2F_{7/2}$ emission of Ce(I) and the $5d \rightarrow {}^2F_{5/2}$ emission of Ce(II). Since the two Sr^{2+} sites have similar coordination polyhedron but the site size of Sr1 is larger than that of Sr2, it is plausible that the Ce(I) emission relates to the larger Sr1 site and the Ce(II) emission relates to the smaller Sr2 site.

Figure 2(b) reveals three broad excitation bands denoted as D (~275 nm), E (~296 nm), and F (~310 nm). They

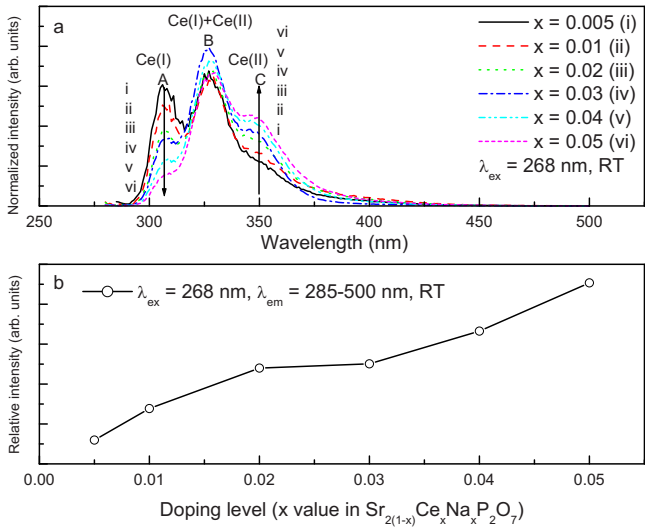

FIG. 3. (Color online) (a) The normalized emission (λ_{ex}=268 nm) spectra of $Sr_{2(1-x)}Ce_xNa_xP_2O_7$ (x=0.005,0.01,0.02,0.03,0.04,0.05) at RT and (b) the integrated emission intensity in the 285–500 nm spectral range as a function of doping concentration (x value) upon 268 nm excitation.

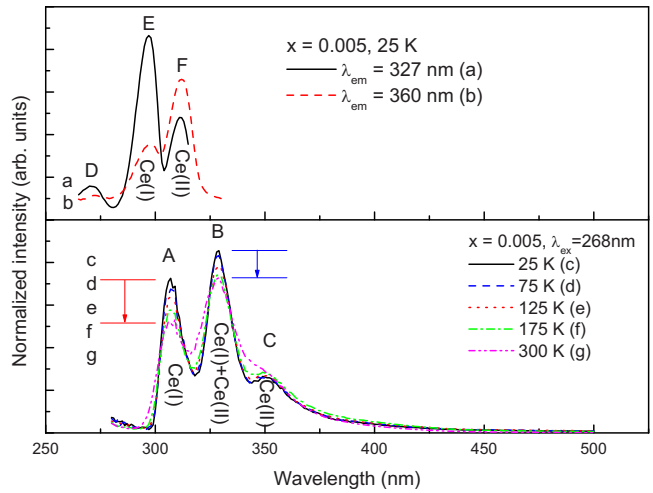

FIG. 4. (Color online) The normalized excitation spectra (λ_{em}=327, 360 nm) at 25 K and the normalized emission spectra (λ_{ex}=268 nm) at different temperature for sample $Sr_{2(1-x)}Ce_xNa_xP_2O_7$ with x=0.005.

correspond to $4f^1 \rightarrow 5d^1$ excitations of Ce^{3+}. As we will show below, band E is due to the transition from the $^2F_{5/2}$ ground state to the lowest $5d$ state of Ce^{3+} located at the larger Sr1 site. Band F is then attributed to the lowest energy $4f-5d$ transition of Ce^{3+} located at the smaller Sr2 site.

C. Influence of Ce^{3+} concentration on luminescence properties

The normalized RT emission (λ_{ex}=268 nm) spectra of $Sr_{2(1-x)}Ce_xNa_xP_2O_7$ with different Ce^{3+} concentration (x =0.005,0.01,0.02,0.03,0.04,0.05) are shown in Fig. 3(a). The same three emission bands A, B, and C are observed as those in Fig. 2(a). The intensity of band A decreases with the increase in doping concentration while that of band C increases. The intensity of band B remains almost invariable except for the sample with x=0.03 where the intensity increases.

We expect that the distribution of Ce^{3+} over the two Sr^{2+} available sites will change with concentration. This together with the energy transfer (ET) between different Ce^{3+} centers, that also will depend on concentration, affects the intensity change in the three emission bands. Let us first assume that at low Ce^{3+} concentration, Ce^{3+} preferentially occupy Sr1 sites, and that the probability of Ce^{3+} occupying the Sr2 sites gradually increases with increasing concentration. In that case, the intensity of band A should be relatively strong for the low-doping samples whereas that of band C should be relatively strong for the high-doping samples. This is just what is observed in the emission spectra.

Another aspect is that ET from Ce(I) on the large Sr1 sites to Ce(II) on the small Sr2 sites is energetically possible. Figure 2 shows that the emission band A of Ce(I) has a strong spectral overlap with the excitation band F of Ce(II). Therefore efficient ET from Ce(I) to Ce(II) is possible especially when the doping concentration increases, and the emission from Ce(II) gradually increases at the expense of that from Ce(I).

In principle, concentration quenching may also influence the emission intensity. However, Fig. 3(b) does not show evidence for concentration quenching. On the contrary, up to x=0.05 the luminescence intensity still increases with x. The low concentration quenching is decided by the structural characteristics of α-$Sr_2P_2O_7$ and the electronic configuration of Ce^{3+}. Because the difference in chemical environment around the two types of Ce^{3+} centers is small, we assume that for both sites concentration quenching does not occur in this doping concentration range.

The intensity of band B is nearly invariable with concentration, except that the sample $Sr_{1.94}Ce_{0.03}Na_{0.03}P_2O_7$ (curve iv) shows a relatively strong intensity. We think that the almost constant intensity relates to the spectral overlap between the $5d \rightarrow {}^2F_{7/2}$ emission of Ce(I) and the $5d \rightarrow {}^2F_{5/2}$ emission of Ce(II) at the position of band B. With increase in doping concentration, the emission from Ce(I) decreases but that from Ce(II) increases. Apparently, the decrease in $5d \rightarrow {}^2F_{7/2}$ emission from Ce(I) is largely compensated by the increase in $5d \rightarrow {}^2F_{5/2}$ emission from Ce(II), thus resulting in a nearly invariable intensity of band B.

D. Influence of temperature on luminescence

Figure 4 shows the normalized excitation spectra (λ_{em} =327, 360 nm) at 25 K and the normalized emission spectra (λ_{ex}=268 nm) at different temperatures for sample $Sr_{2(1-x)}Ce_xNa_xP_2O_7$ with x=0.005. By monitoring different emission wavelengths, we recorded two excitation spectra as shown in Figs. 4(a) and 4(b). Monitoring 327 nm emission, the excitation band E at ~297 nm shows the strongest intensity. When monitoring 360 nm, excitation band F at ~312 nm has strongest intensity. These results further confirm that bands E and F are the lowest energy $4f-5d$ excitations of Ce(I) and Ce(II), respectively.

In the emission spectra of Figs. 4(c)–4(g), we observe again the three emission bands A (~307 nm), B (~329 nm), and C (~349 nm). When we assign the lowest energy $4f-5d$ excitation bands at ~297 (band E) and ~312 nm (band F) to Ce(I) and Ce(II) centers, respectively,

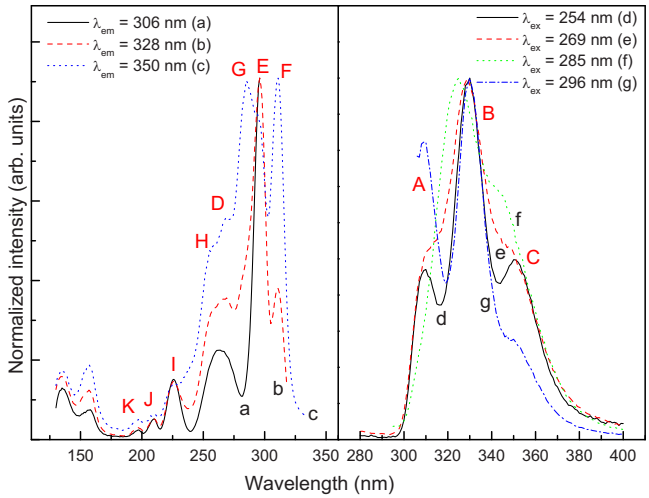

FIG. 5. (Color online) The VUV-UV excitation spectra and corresponding emission spectra of sample α-$Sr_{2-2x}Ce_xNa_xP_2O_7$ (x=0.005) at 13 K.

then the Stokes shifts in Ce(I) and Ce(II) emission are ~1096 cm^{-1} and ~1656 cm^{-1}, respectively. These values are somewhat smaller than the average Stokes shift in about 2500 cm^{-1} observed for Ce^{3+} emission in compounds. This suggests a relatively weak 5*d* electron phonon coupling in the host lattice.[1]

When the intensity of bands A–C in Figs. 4(c)–4(g) is compared each other, one observes that the intensities of bands A and B decrease with temperature increase. Band A decreases more rapidly than band B. The intensity of band C remains nearly constant. The ET from Ce(I) to Ce(II) may be responsible for this phenomenon. With increase in temperature, both the emission and the excitation bands broaden. The increase in spectral overlap will then augment the Ce(I) →Ce(II) ET efficiency. Therefore, band A decrease most rapidly because it is Ce(I) emission, band B decrease less rapidly because it is both Ce(I) and Ce(II) emission. With this reasoning the intensity of the Ce(II) emission band C is expected to increase somewhat. This was not observed and that may be due to thermal-quenching effects.

E. VUV spectra and influence of excitation wavelength on luminescence

VUV-UV excitation spectra and corresponding emission spectra of sample $Sr_{2-2x}Ce_xNa_xP_2O_7$ (x=0.005) were measured at 13 K at BSRF, and the results are shown in Fig. 5. In order to reveal changes in band intensity, we have normalized the spectra to the height of the strongest band in each spectrum.

In Figs. 5(a)–5(c), the excitation of the host lattice is observed in the spectral range below 180 nm. The excitation onset is at ~170 nm and it is followed by two excitation maxima at ~158 and ~136 nm. Usually the excitation of the phosphate group is located around 150–170 nm.[12,16,17] The weak intensity of the host-related excitation bands indicates an inefficient ET from the host lattice to Ce^{3+} ions. Above 180 nm, eight $4f \rightarrow 5d$ excitation bands of Ce^{3+} at ~196 nm (K), ~210 nm (J), ~225 nm (I), ~254 nm (H), ~269 nm (D), ~285 nm (G), ~296 nm (E), and ~310 nm (F) are observed. Because Ce^{3+} may enter two different C_s-symmetry Sr^{2+} sites, at most ten crystal field split 5*d* excitation bands can be expected. Therefore still two are missing. Probably some of the 5*d* excitation bands overlap each other and cannot be resolved in the excitation spectra.

Band E at ~296 nm and band F at ~310 nm in Figs. 5(a) and 5(b) were already assigned to the first $4f \rightarrow 5d$ excitation bands of Ce(I) and Ce(II), respectively. When we move the monitoring emission wavelength from the Ce(II) 350 nm band to the Ce(I)+Ce(II) 328 nm band, the F/E band intensity ratio decreases. This is in agreement with what can be observed in the upper panel of Fig. 4. Band G at ~285 nm is most likely the second 5*d* excitation band of Ce(II), because it can also be clearly observed in Fig. 5 spectrum (c) when the emission from Ce(II) at 350 nm is monitored. When the monitoring wavelength shifts first to the 328 nm emission from Ce(I)+Ce(II) and then to the 306 nm emission from Ce(I), its intensity decreases progressively. This band G cannot be resolved in Fig. 4. Possibly it is hidden in the tail of band E. Also the low resolution and the weak sensitivity of the UV spectrometer in this range may prevent its detection. The other five bands D, H, I, J, K with higher energies cannot be unambiguously assigned to specific Ce^{3+} centers.

Spectrum (g) in Fig. 5 shows that upon 296 nm excitation in the E-band, the emission intensity of band A is stronger and that of band C is weaker than when excitation is at another wavelength. However, upon 285 nm excitation in band G, the emission intensity of band C is strong and the emission intensity of band A is weak. These observations confirm our assignments for bands G and E as belonging to Ce(II) and Ce(I) centers. Upon excitation at 254 nm in band H and at 269 nm in band D, the emission from Ce^{3+} at both sites can be observed due to the spectral overlap ET between these higher 5*d* excited states occurs.

An interesting phenomenon is the peak position of emission band B. This band B shows a maximum at ~330 nm at 296 nm band E excitation. The maximum shifts to ~325 nm upon 285 nm band G excitation. Because band G is assigned to Ce(II) excitation, the emission mainly comes from Ce^{3+} at Sr2 sites. This result indicates that the $5d \rightarrow {}^2F_{5/2}$ emission of Ce(II) is at the short-wavelength side of band B, while the $5d \rightarrow {}^2F_{7/2}$ emission of Ce(I) is at the long-wavelength side of band B.

F. Luminescence decay characteristics

The luminescence decay spectra were measured for all samples $Sr_{2(1-x)}Ce_xNa_xP_2O_7$ at RT, and typical results for x =0.005, 0.03, and 0.05 are displayed in Fig. 6. Upon excitation of band E at 297 nm and monitoring band A emission at 306 nm, we obtained the luminescence decay curves of Ce(I) centers as shown in Fig. 6(a). These curves can be well fitted using a single exponential equation, $I_t = I_0 \exp(-t/\tau)$, where I_t and I_0 are the luminescence intensities at time t and at time t=0, and τ is the decay constant. We obtained decay constants $\tau_{1/e} \approx 17.7$ ns, 12.9 ns, and 11.6 ns for x=0.005, 0.03, and 0.05, respectively. When the doping concentration increases, the decay constant of Ce(I) centers clearly shortens

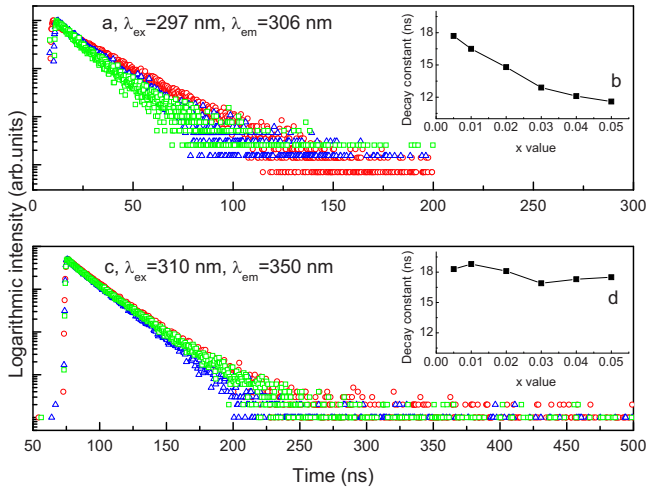

FIG. 6. (Color online) Luminescence decay spectra of samples $Sr_{2(1-x)}Ce_xNa_xP_2O_7$ for x=0.005 (red circle line), 0.03 (blue triangle line), and 0.05 (green square line) at RT, the insets b and d show the decay constants (λ_{ex}=297 nm, λ_{em}=306 nm; λ_{ex}=310 nm, λ_{em}=350 nm) as a function of doping content (x value).

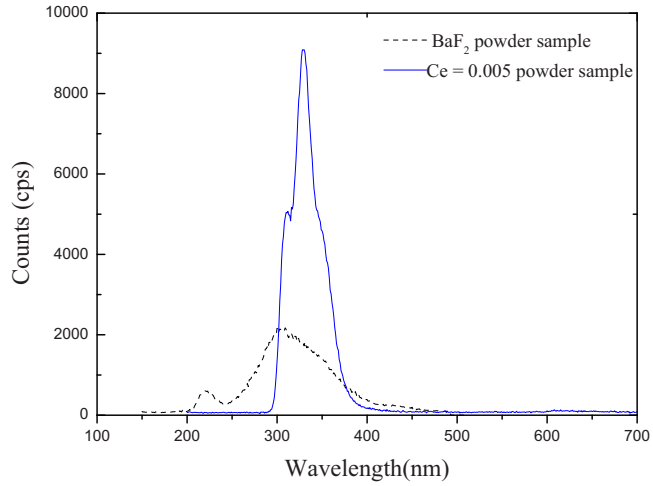

FIG. 7. (Color online) X-ray excited emission spectra of α-$Sr_{1.99}Ce_{0.005}Na_{0.005}P_2O_7$ and BaF_2 powder at RT.

as shown in Fig. 6(b). This confirms that the ET rate from Ce(I) to Ce(II) increases with Ce concentration.

Under excitation of band F at 310 nm and monitoring band C emission at 350 nm, we obtained the luminescence decay spectra of Ce(II) as shown in Fig. 6(c). The phosphors still exhibit exponential decay but the decay constant around 17.8 ns is hardly influenced by the doping concentration as shown in Fig. 6(d). This observation is consistent with our earlier observation that concentration quenching of Ce(II) luminescence is not of much significance in the investigated concentration range.

G. Luminescence under x-ray excitation

The x-ray excited luminescence spectrum of α-$Sr_{2(1-x)}Ce_xNa_xP_2O_7$ (x=0.005) was recorded using a Philips PW2253/20 X-ray tube with Cu anode operating at 60 kV and 25 mA. BaF_2 powder with well known properties was used as a reference sample to obtain an estimate for the absolute emission intensity from our samples. The results are shown in Fig. 7. The emission shows again the three bands at 310, 330, and 350 nm due to the $5d \rightarrow 4f$ transitions of Ce^{3+} ions at the two available Sr^{2+} sites. From the known absolute total light yield of 8880 photons/MeV of absorbed x-ray energy for the BaF_2 reference sample, the x-ray excited light yield of $Sr_{2(1-x)}Ce_xNa_xP_2O_7$ (x=0.005) is estimated to be around 10 000 photons/MeV.

IV. CONCLUSIONS

The luminescence properties of Ce^{3+} doped α-$Sr_{2-2x}Ce_xNa_xP_2O_7$ phosphors were investigated under VUV-UV and x-ray excitation. It was found that Ce^{3+} ions enter two different sites in the host lattice. Ce(I) centers are the ones on the larger Sr1 sites, and they show the lowest energy 5*d* excitation band around 296 nm with the doublet emission bands at about 310 and 330 nm. Ce(II) centers at the smaller Sr2 sites have the first and the second 5*d* excitation bands around 311 nm and 285 nm with the doublet emission bands around 330 and 350 nm. At RT, the decay constant $\tau_{1/e}$ for Ce(I) centers is about 17.7 ns for the sample with x=0.005, and this value decreases with the increase in doping concentration due to Ce(I)→Ce(II) ET. Ce(II) centers exhibit a nearly invariable decay time around 17.8 ns. Because the distribution of Ce over the available sites changes with concentration and because of energy transfer from Ce(I) to Ce(II) centers, the luminescence from Ce(II) centers increase at the expense of that from Ce(I) centers with increase in Ce^{3+} concentration. In addition, an increased energy transfer efficiency results in a decrease in the $5d \rightarrow {}^2F_{5/2}$ emission intensity of Ce(I) with temperature increase. The intensity of Ce(II) $5d \rightarrow {}^2F_{7/2}$ emission is nearly invariable with concentration. The x-ray excited light yield of sample α-$Sr_{2(1-x)}Ce_xNa_xP_2O_7$ (x=0.005) is estimated about 10 000 photons/MeV.

ACKNOWLEDGMENTS

This work is funded by the National Basic Research Program of China (973 Program, Grant No. 2007CB935502), by the National Natural Science Foundation of China (Grant Nos. 20871121 and 10979027), and by the Natural Science Foundation of Guangdong Province (Grant No. 9151027501000003).

[1]P. Dorenbos, Phys. Rev. B **64**, 125117 (2001).
[2]C.-K. Chang and T.-M. Chen, Appl. Phys. Lett. **91**, 081902 (2007).
[3]C. F. Guo, L. Luan, Y. Xu, F. Gao, and L. F. Liang, J. Electrochem. Soc. **155**, J310 (2008).
[4]V. Bachmann, C. Ronda, and A. Meijerink, Chem. Mater. **21**, 2077 (2009).
[5]W. B. Im, S. Brinkley, J. Hu, A. Mikhailovsky, S. P. DenBaars, and R. Seshadri, Chem. Mater. **22**, 2842 (2010).
[6]Y. H. Song, H. P. You, M. Yang, Y. H. Zheng, K. Liu, G. Jia, Y. J. Huang, L. H. Zhang, and H. J. Zhang, Inorg. Chem. **49**, 1674 (2010).
[7]K.V. Ivanovskikh, A. Meijerink, F. Piccinelli, A. Speghini, E.I. Zinin, C. Ronda, and M. Bettinelli, J. Lumin. **130**, 893 (2010).
[8]G. Blasse and B. C. Grabmeyer, *Luminescent Materials* (Springer, Berlin, 1994).
[9]S. Ye, Z.-S. Liu, J.-G. Wang, and X.-P. Jing, Mater. Res. Bull. **43**, 1057 (2008).
[10]R. Pang, C. Y. Li, L. L. Shi, and Q. Su, J. Phys. Chem. Solids **70**, 303 (2009).
[11]Y. Tao, Y. Huang, Z. H. Gao, H. Zhuang, A. Y. Zhou, Y. L. Tan, D. W. Li,

and S. S. Sun, J. Synchrotron Radiat. **16**, 857 (2009).
[12]Q. Zeng, H. B. Liang, G. B. Zhang, M. D. Birowosuto, Z. F. Tian, H. H. Lin, Y. B. Fu, P. Dorenbos, and Q. Su, J. Phys.: Condens. Matter **18**, 9549 (2006).
[13]C. W. W. Hoffman and R. W. Mooney, J. Electrochem. Soc. **107**, 854 (1960).
[14]L. Hagman, I. Jansson, and C. Magneli, Acta Chem. Scand. **22**, 1419 (1968).
[15]J. Barbier and J.-P. Echard, Acta Crystallogr., Sect. C: Cryst. Struct. Commun. **54**, IUC9800070 (1998).
[16]J. P. Zhong, H. B. Liang, H. H. Lin, B. Han, Q. Su, and G. B. Zhang, J. Mater. Chem. **17**, 4679 (2007).
[17]Z. F. Tian, H. B. Liang, B. Han, Q. Su, Y. Tao, G. B. Zhang, and Y. B. Fu, J. Phys. Chem. C **112**, 12524 (2008).